

# Screening of Oxygen Evolution Electrocatalysts by Scanning Electrochemical Microscopy Using a Shielded Tip Approach

Alessandro Minguzzi,<sup>†</sup> Mario A. Alpuche-Aviles,<sup>\*,§</sup> Joaquin Rodríguez López,<sup>‡</sup> Sandra Rondinini,<sup>†</sup> and Allen J. Bard<sup>\*,‡</sup>

Department of Physical-Chemistry and Electrochemistry, University of Milan, via Golgi 19, 20133 Milan, Italy, and  
Department of Chemistry and Biochemistry, Center for Electrochemistry, University of Texas at Austin, Austin, Texas 78712

Oxygen evolution electrocatalysts in acidic media were studied by scanning electrochemical microscopy (SECM) in the substrate generation–tip collection (SG–TC) imaging mode with a 100  $\mu\text{m}$  diam tip. Pure  $\text{IrO}_2$  and  $\text{Sn}_{1-x}\text{Ir}_x\text{O}_2$  combinatorial mixtures were prepared by a sol–gel route to form arrays of electrocatalyst spots. The experimental setup has been developed to optimize screening of electrocatalyst libraries under conditions where the entire array is capable of the oxygen evolution reaction (OER). The activity of individual spots was determined by reducing the interference from the reaction products of neighboring spots diffusing to the tip over the spot of interest. A gold layer deposited on the external wall of the SECM tip was used as a tip shield. In this study the shield was kept at a constant potential to reduce oxygen under mass transfer controlled conditions. The tip shield consumes oxygen coming from the neighbor spots in the array and enables the tip to correctly detect the activity of the spot below the tip. Simulations and experimental results are shown, demonstrating the effectiveness of the tip shield with the SG–TC setup in determining the properties of the composite materials and imaging arrays.

Mixtures of Ir/Sn binary oxides with different compositions were evaluated as electrocatalysts for the oxygen evolution reaction (OER) with the scanning electrochemical microscope (SECM). The substrate generation–tip collection mode (SG–TC) was used with a tip shielding method to screen an array of electrocatalytic spots of different compositions as a function of potential. The tip measures the oxygen produced at the electrocatalyst test spot, with a spot that electrolyzes water at the least positive potential to produce oxygen considered the most efficient. The tip shield method allows one to determine the activity of individual spots for the OER when neighboring spots in the array also generate oxygen. The OER is one of the most studied reactions in electrocatalysis since it is involved in many electrochemical industrial processes (cathodic protection, water electrolysis, metal recovery, photoelectrochemical water oxidation)

and its kinetics limits the entire electrolysis process, since it is considerably slower than most cathodic processes.<sup>1–5</sup> If the reaction is conducted in acidic media, the list of anode materials is restricted to  $\text{IrO}_2$  and  $\text{RuO}_2$  because of their high activity and chemical resistance under the operating conditions.<sup>6</sup>  $\text{RuO}_2$  shows the higher activity, but  $\text{IrO}_2$  lasts about 20 times longer and thus is more interesting from an industrial point of view.<sup>7</sup>

The high cost of  $\text{IrO}_2$  has motivated researchers to obtain a suitable composite material:  $\text{IrO}_2$  must be dispersed in an inexpensive, but stable, matrix. Many factors can influence the properties of the material, mainly its composition and the preparation technique, and there is an extensive literature on this topic. In particular, the material composition, i.e., the nature of the dispersing agent and its ratio to the  $\text{IrO}_2$ , is still being investigated and discussed. Recently, several mixed oxide systems have been studied:  $\text{IrO}_2 + \text{SnO}_2$ ,<sup>8–11</sup>  $\text{IrO}_2 + \text{Ta}_2\text{O}_5$ ,<sup>12–21</sup>  $\text{IrO}_2 + \text{SnO}_2 +$

- (1) Katsounis, A.; Brosda, S.; Vayenas, C. G. In *Encyclopedia of Electrochemistry*; Bard, A. J., Stratmann, M., Eds.; Wiley-VCH Verlag GmbH & Co. KGaA: Weinheim, Germany, 2007; Vol. 5.
- (2) Schiffrin, D. J. In *Electrochemistry, Chapter 4, Specialist Periodical Reports*; The Royal Society of Chemistry: London, 1983; Vol. 8.
- (3) Appleby, A. J. In *Comprehensive Treatise of Electrochemistry*; Conway, B. E., Ed.; Plenum: New York, 1983; Vol. 7, pp 173–239.
- (4) Tarasevich, M. R.; Sadkowsky, A.; Yeager, E. In *Comprehensive Treatise of Electrochemistry*; Conway, B. E., Ed.; Plenum: New York, 1983; Vol. 7, pp 301–398.
- (5) Herrero, E.; Feliu, J. M.; Aldaz, A. In *Encyclopedia of Electrochemistry*; Bard, A. J., Stratmann, M., Eds.; Wiley-VCH Verlag GmbH & Co. KGaA: Weinheim, Germany, 2007; Vol. 2.
- (6) Trasatti, S. In *Electrodes of Conductive Metallic Oxides, Part B*; Trasatti, S., Ed.; Elsevier: Amsterdam, 1980; pp 521–626.
- (7) Alves, V. A.; Da Silva, L. A.; Oliveira, E. D.; Boodts, J. F. C. *Mater. Sci. Forum* **1998**, *655*, 289–292.
- (8) Balko, E. N.; Nguyen, P. H. *J. Appl. Electrochem.* **1991**, *21*, 678–682.
- (9) De Pauli, C. P.; Trasatti, S. *J. Electroanal. Chem.* **1995**, *396*, 161.
- (10) De Pauli, C. P.; Trasatti, S. *J. Electroanal. Chem.* **2002**, *538*, 145.
- (11) Marshall, A.; Børresen, B.; Hagen, G.; Tsyppkin, M.; Tunold, R. *Electrochim. Acta* **2006**, *51*, 3161–3167.
- (12) Comninellis, C.; Vercesi, G. P. *J. Appl. Electrochem.* **1991**, *21*, 335.
- (13) Comninellis, C.; Vercesi, P. *J. Appl. Electrochem.* **1991**, *21*, 139.
- (14) Xu, L. K.; Scantlebury, J. D. *J. Electrochem. Soc.* **2003**, *150*, B254.
- (15) Xu, L. K.; Scantlebury, J. D. *J. Electrochem. Soc.* **2003**, *150*, B288.
- (16) Hu, J. M.; Zhang, J. Q.; Meng, H. M.; Cao, C. N. *J. Mater. Sci.* **2003**, *38*, 705.
- (17) Hu, J. M.; Meng, H. M.; Zhang, J. Q.; Cao, C. N. *Corros. Sci.* **2002**, *44*, 1655.
- (18) Hu, J. M.; Zhang, J. Q.; Cao, C. N. *Int. J. Hydrogen Energy* **2004**, *29*, 791.
- (19) Morimitsu, M.; Otagawa, R.; Matsunaga, M. *Electrochim. Acta* **2000**, *46*, 401.
- (20) Rasten, E. Ph.D. Thesis, NTNU Trondheim, Norway, 2001.

\* Corresponding author. E-mail: ajbard@mail.utexas.edu.

<sup>†</sup> University of Milan.

<sup>‡</sup> University of Texas at Austin.

<sup>§</sup> Current address: Department of Chemistry, The Ohio State University, Columbus, Ohio 43210.

Ta<sub>2</sub>O<sub>5</sub>,<sup>22</sup> IrO<sub>2</sub> + Sb<sub>2</sub>O<sub>5</sub> + SnO<sub>2</sub>,<sup>23,24</sup> with the aim of improving both the stability and the electroactivity of the catalyst, by taking advantage of the synergistic effects that could occur in a nanostructured matrix.

De Pauli and Trasatti<sup>9,10</sup> showed that SnO<sub>2</sub> + IrO<sub>2</sub> mixtures prepared by thermal decomposition of the precursor salts show the same (or slightly higher) activity than the pure IrO<sub>2</sub> in the 20–70% w/w IrO<sub>2</sub> content window. The same behavior was not observed by other authors,<sup>8,11</sup> who claim an increase of activity with the iridium content. A recent paper reported that the doping on SnO<sub>2</sub> + IrO<sub>2</sub> mixtures with Ta<sub>2</sub>O<sub>5</sub> leads to a general improvement of the material performance mainly due to an increase of surface area, and consequently of catalyst accessibility, with respect to the SnO<sub>2</sub> + IrO<sub>2</sub> system.<sup>22</sup> In other cases, a dispersing agent was reported to extend the life of the electrocatalysts, e.g., IrO<sub>2</sub> + Sb<sub>2</sub>O<sub>5</sub> + SnO<sub>2</sub> mixtures.<sup>23,24</sup>

A technique, like SECM, that allows the rapid evaluation of composite material activity as a function of composition, at least as a first approach, is useful in generating potentially useful electrocatalysts for the OER. SECM has already demonstrated its screening capabilities in the case of the oxygen reduction reaction (ORR).<sup>25,26</sup> In this technique, an array of spots 100–400 μm in diameter of different compositions is prepared over an inert (glassy carbon) substrate. The electrocatalytic activity of the different compositions is studied in a single imaging experiment with the tip generation–substrate collection (TG–SC) mode (with the tip generating oxygen and the substrate spot reducing it). A plot of the substrate current as a function of tip position corresponds to an image of the catalytic activity of the spots at a given potential. Since the solution is deaerated, when the oxygen-generating tip passes over an active spot for ORR, the substrate current increases from that of the background; more active spots produce higher collection currents at lower overpotentials as a result of more facile kinetics.<sup>27</sup>

The TG–SC mode cannot work for the OER, since water, the reactant, is already present throughout the sample solution. However, an SG–TC approach can be used. Our experimental scheme is shown in Figure 1. This approach is analogous to the combinatorial studies of ORR electrocatalysts: the experiment consists in recording the current of an amperometric sensing tip (a 100 μm diameter tip, with ultra-micro-electrode (UME)-like behavior, placed at a potential negative enough to reduce oxygen under mass transfer limiting conditions) as a function of its position while scanning an array of spots of different compositions kept under OER conditions at constant potential. In this case a sufficiently high potential is applied to the substrate while the tip works as an amperometric sensor reducing the oxygen produced by spots of the array.

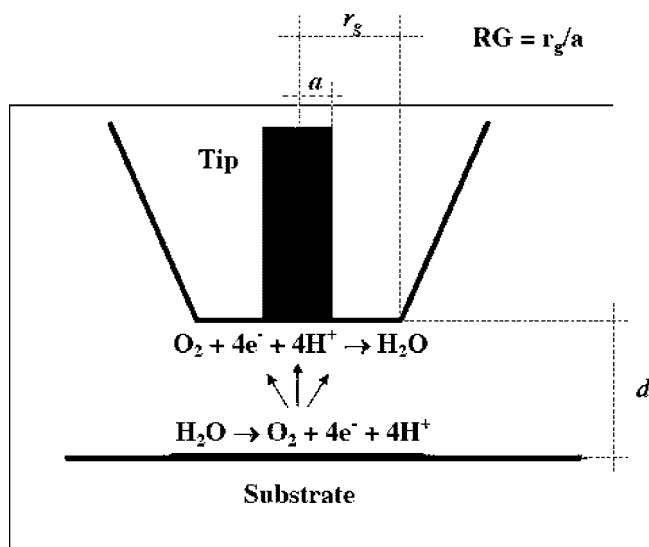


**Figure 1.** Schematic representation of the electrochemical processes involved in an SG–TC experiment in which oxygen is evolved at the substrate and reduced at the tip.

For quantitative or semiquantitative measurements, it is important to reach the highest possible collection efficiency (CE), defined as the ratio of the current flowing through one spot to the current flowing through the tip. This can be approached by using a tip with a sufficiently large radius,  $a$ , provided that it still behaves essentially like a UME. Obtaining high CE values in the SG–TC mode is more difficult compared to the TG–SC one, since the spots prepared typically have larger radii than the tip.<sup>28</sup> In this article, we will show the results obtained using a 100 μm diam Au tip and its application to the preliminary characterization of mixed oxide electrocatalysts for OER.

The selection of the RG value (the ratio between the radius of the glass surrounding the tip to the tip electrode radius) is also a critical parameter. The higher the RG, the higher the collection efficiency, since a smaller amount of the oxygen produced by the substrate spot is able to escape into the solution. However a large RG makes the tip harder to use, since, even with a good tip–substrate alignment, it becomes easier to scratch the substrate during imaging experiments. In our case, a value of  $RG = 4$  resulted to be a good compromise.

When using the SG–TC mode in screening experiments, the overlap of diffusion layers of neighboring spots usually complicates the analysis, unless the distance between the edges of the spots (typically 200–300 μm) is extremely high (>1 mm). However, increasing the distance between spots is not always feasible since it lengthens the time to scan an array. When the spots diffusion layers overlap, the tip current is a function of the amount of O<sub>2</sub> produced by both the spot under investigation and also by O<sub>2</sub> from the neighboring spots, thus misrepresenting the activity of the electrocatalytic spot. This is particularly troublesome when the tip is over less active spots, i.e., when the amount O<sub>2</sub> generated by one spot is comparable to O<sub>2</sub> coming from its neighborhood. This results also in high background currents, thus reducing the signal-to-noise ratio, the image contrast, and compromising the screening resolution.

(21) Da Silva, L. M.; Franco, D. V.; De Faria, L. A.; Boodts, J. F. C. *Electrochim. Acta* **2004**, *49*, 3977.

(22) Ardizzone, S.; Bianchi, C. L.; Cappelletti, G.; Ionita, M.; Minguzzi, A.; Rondinini, S.; Vertova, A. J. *Electroanal. Chem.* **2006**, *589*, 160–166.

(23) Chen, X.; Chen, G.; Yue, P. L. *J. Phys. Chem. B* **2001**, *105*, 4623.

(24) Chen, G.; Chen, X.; Yue, P. L. *J. Phys. Chem. B* **2002**, *106*, 4364.

(25) Fernández, J. L.; Walsh, D. A.; Bard, A. J. *J. Am. Chem. Soc.* **2005**, *127*, 357–365.

(26) Fernández, J. L.; Raghuvveer, V.; Manthiram, A.; Bard, A. J. *J. Am. Chem. Soc.* **2005**, *127*, 13100.

(27) Fernández, J. L.; Bard, A. J. *Anal. Chem.* **2003**, *76*, 2281.

(28) Bard, A. J. In *Scanning Electrochemical Microscopy*; Bard, A. J., Mirkin, M. V., Eds.; Marcel Dekker Inc.: New York, 2001; pp 1–16.

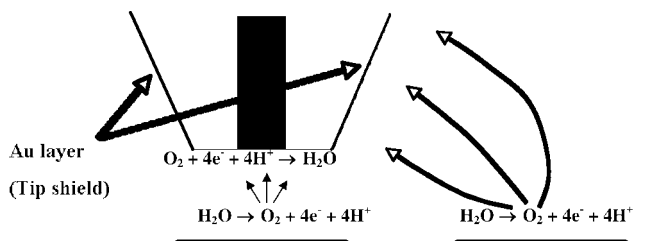


**Figure 2.** Schematic representation of the tip shield approach: the tip reduces only oxygen coming from the spot under investigation while oxygen coming from neighboring spots is reduced at the tip shield.

To minimize the effects of the neighboring spots, we chose to shield the tip from the oxygen coming from neighboring spots by reducing it at the tip wall. To this end the tip walls were modified by coating it by vacuum evaporation with a Au layer that was held at a potential where any oxygen reaching this coating was reduced at mass transfer limiting conditions as shown in Figure 2. Although other approaches to this problem are possible, e.g., degassing the solution or continuously replacing it to keep the dissolved  $\text{O}_2$  concentration low, the possibility of introducing a convective component to the tip current, as well as technical complications, e.g., the use of a flow-cell, make the tip shield approach the most straightforward.

In this article, the use of a tip shielding approach in the SG–TC mode of SECM is presented. The use of this setup to screen electrocatalysts for the OER is demonstrated. Simulations and experimental results are used to establish the effectiveness of this method. Different arrays have been examined, consisting in either 100%  $\text{IrO}_2$  (sample a) or in  $\text{Sn}_{1-x}\text{Ir}_x\text{O}_2$  mixtures (sample b) with  $x$  varying from 1 to 0. In addition, two larger electrodes (samples c, 100% Ir, and d, 60% Ir), supported on a Ti plate, were prepared, by the same preparation procedure at the two specific single compositions, and tested by means of slow potentiodynamic curves. The results with these electrodes are in accord with the trend in electrocatalytic activity found with the tip shield in the SECM SG–TC mode. All the spots were prepared using a sol–gel technique, starting from the chloride salts.

## EXPERIMENTAL SECTION

All chemicals were used as received. Aqueous solutions were prepared with water from a Millipore purification system. All the experiments were performed at room temperature.

**Sample Preparation.** Array (a) consists of nine  $\text{IrO}_2$  spots arranged as a  $3 \times 3$  grid. The distance between spot centers was set at  $1000 \mu\text{m}$ . A solution of  $0.1 \text{ M IrCl}_3 \cdot 3\text{H}_2\text{O}$  (99.8% purity, Alfa Aesar, Ward Hill, MA) in ethylene glycol was dispensed on Ti foil ( $1.5 \times 1.5 \text{ cm}^2$ ,  $0.75 \text{ mm}$  thickness, 99.7% purity, Aldrich, St. Louis, MO, previously washed in water and sonicated in acetone) using a CHI 1550 picoliter dispenser (CH Instruments, Austin, TX) and applying the following parameters: number of drops per spot, 10; pulse amplitude,  $80 \text{ V}$ ; pulse width,  $40 \mu\text{s}$ ; pulse period,  $1000 \text{ ms}$ .

The samples were aged in air for 24 h, then dried for 1 h at  $180 \text{ }^\circ\text{C}$  (after a  $5 \text{ }^\circ\text{C}/\text{min}$  ramp) in a tube furnace under an Ar flow. They were annealed at  $500 \text{ }^\circ\text{C}$  for 2 h in oxygen (1 atm). During the cooling period, samples were kept under Ar. In this procedure,  $350 \mu\text{m}$  diam spots were obtained.

For array (b), spots based on  $\text{Sn}_{1-x}\text{Ir}_x\text{O}_2$  mixed oxides in the nominal composition range from 0% to 100% of  $\text{IrO}_2$  have been prepared in 10% ( $\Delta x = 0.1$ ) increments. A solution of  $0.1 \text{ M IrCl}_3 \cdot 3\text{H}_2\text{O}$  in water/glycerol (3:1) was first dispensed on Ti foil as in the previous case, with the following spot deposition parameters: pulse amplitude,  $50 \text{ V}$ ; pulse width,  $15 \mu\text{s}$ ; pulse period,  $500 \text{ ms}$ ; center-to-center distance,  $500 \mu\text{m}$ , while the number of drops in each column were changed from 10 to 0 in the  $y$  direction. Successively, a  $0.1 \text{ M}$  solution of  $\text{SnCl}_4 \cdot 5\text{H}_2\text{O}$  (98% purity Alfa Aesar, Ward Hill, MA) in water/glycerol (3:1) was dispensed in the same way as for the Ir precursor. To keep the total moles of the two components constant on every spot, the number of drops is varied between 0 and 10. In this way 11  $\text{Sn}_{1-x}\text{Ir}_x\text{O}_2$  spots were obtained with nominal compositions ranging from  $x = 1$  (100%  $\text{IrO}_2$ ) to  $x = 0$  (100%  $\text{SnO}_2$ ) with steps of  $\Delta x = 0.1$ . The array consisted of an  $11 \times 3$  grid (three equivalent spot lines to study reproducibility). The sample was vortexed for 10 min and immediately exposed to gaseous  $\text{NH}_3$  (1 atm) for 1 h. Then the sample was aged, dried, and annealed using the same procedure as followed for array (a). This procedure yielded  $300 \mu\text{m}$  diam spots.

Two samples were also prepared using  $0.1 \text{ M IrCl}_3 \cdot 3\text{H}_2\text{O}$  and  $\text{IrCl}_3 \cdot 3\text{H}_2\text{O}/\text{SnCl}_4 \cdot 5\text{H}_2\text{O}$  6:4, solutions in water/glycerol 3:1, respectively. For each electrode  $1 \mu\text{L}$  drop was dispensed on the same Ti lamina support used in the array preparation in order to have a large surface area. The samples were then treated in the same way as for all the other samples. At the end of the procedure a 100% (sample c) and a 60% Ir (sample d) containing spot, respectively, were obtained.

**Tip Preparation.** A  $100 \mu\text{m}$  diam gold wire (Goodfellow, 99.99% purity) was sealed into a flint glass capillary o.d./i.d.  $1.5/0.75 \text{ mm}$  (no. 27-37-1, Frederik Haer & Co, Bowdoinham, ME) under vacuum. One end was then polished with 600 mesh sandpaper (Buehler, Lake Bluff, IL) until the metal disk was exposed, then smoothed with 1200 mesh abrasive SiC paper and alumina suspensions in water down to  $0.3 \mu\text{m}$  (Buehler). Finally, the tip was sharpened, reaching an RG of 4.

The tip wall was further modified by covering it with a gold layer. Two different procedures were tested. The first one consists in the application of a layer of (3-mercaptopropyl)trimethoxysilane (Alfa Aesar, 95%) as reported by Goss et al.<sup>29</sup> followed by Au vapor deposition, carried out in a Denton vacuum DV-502A (Moorestown, NJ) metal evaporator (operating at  $2\text{--}3 \times 10^{-6}$  Torr) equipped with a quartz crystal microbalance (Inficon XTM/2 deposition monitor) to monitor the deposited metal thickness. Electric motors were used to rotate the electrodes during the depositions. At the end of the procedure a nominal gold thickness of  $467 \text{ \AA}$  was obtained (rate  $0.3 \text{ \AA s}^{-1}$ ).

In the second procedure an intermediate layer of  $30 \text{ \AA}$  of Ti (99.7% purity, Aldrich, St. Louis, MO) was deposited on the glass (previously cleaned in 1:4  $\text{H}_2\text{O}_2/\text{concentrated H}_2\text{SO}_4$ , as in the previous method) before depositing  $370 \text{ \AA}$  of gold (rate,  $0.3 \text{ \AA s}^{-1}$ ), as described above. Both of the methods produced homogeneous and coherent adhesion, but the silanization method was preferred because it resulted in a more stable Au coating. Silver epoxy (Epotek H20E, Epoxy Technology, Billerica, MA.) cured overnight at  $100 \text{ }^\circ\text{C}$  was used to make electric contact between the gold

(29) Goss, C. A.; Charych, D. H.; Majda, M. *Anal. Chem.* **1991**, *63*, 85–88.

wire and a copper wire (used as a current collector). Finally, the tip–surface was polished to remove contaminants deposited during the gold layer deposition, using a 0.3  $\mu\text{m}$  alumina powder suspension on an adhesive tape supported on a hard, smooth surface.

**Cyclic Voltammetry.** Cyclic voltammetry (CV) experiments were performed with a CHI 900 SECM workstation (CH Instruments, Austin, TX). Each tip was tested by CV in ferrocenemethanol (FcMeOH, 97%, Aldrich, St. Louis, MO), with a 1 mM solution in aqueous 0.1 M KCl using a silver wire as a quasireference/counter electrode, and in  $\text{O}_2$ -, air-, and Ar-saturated 0.5 M  $\text{H}_2\text{SO}_4$  aqueous solutions using a tungsten wire and a reversible hydrogen electrode (RHE, made with a Pt wire in 0.5 M  $\text{H}_2\text{SO}_4$  saturated with 1 atm  $\text{H}_2$ ) as counter and reference electrodes, respectively.

Single-spot samples (c and d) were characterized by slow potentiodynamic experiments (scanning rate 0.167  $\text{mV s}^{-1}$ ) in an aqueous air-saturated 0.5 M  $\text{H}_2\text{SO}_4$  solution using a tungsten wire and an RHE (made with a Pt wire in 0.5 M  $\text{H}_2\text{SO}_4$  saturated with 1 atm  $\text{H}_2$ ) as counter and reference electrodes, respectively. Samples were placed on the top of a rigid Cu plate and laid on a flat acrylic base. A PTFE cell with a 5 mm diameter orifice in the center was tightened to the acrylic base using an O-ring to surround the array and avoid solution leaking.

**Scanning Electrochemical Microscopy SG–TC Imaging.** The SG–TC mode with the tip shield required the use of both the bipotentiostat of the SECM (CHI 900b with stepper motors, CH Instruments) for the 100  $\mu\text{m}$  diam Au tip and the substrate; a separate potentiostat (CHI600, CH Instruments) was used to control the Au shield layer potential. All measurements were performed in 0.5 M  $\text{H}_2\text{SO}_4$  aqueous solution (not degassed, i.e., in equilibrium with air) using a tungsten wire as the counter electrode and an RHE (made with a Pt wire in a separate borosilicate capillary glass with a soft glass cracked junction filled with 0.5 M  $\text{H}_2\text{SO}_4$  and saturated with 1 atm  $\text{H}_2$  obtained by electrogeneration)<sup>25</sup> as the reference electrode. A separate set of counter and reference electrodes was used for the SECM and the shield potentiostat. When a second 100  $\mu\text{m}$  diam Au tip was used as a substrate, it was held inside a PTFE cell containing 0.5 M  $\text{H}_2\text{SO}_4$  aqueous solution. The tip current was kept constant (370 nA) using a 9 V battery and a resistor.

For array imaging experiments, the sample substrate was placed on the top of a rigid Cu plate laid on a flat acrylic base to provide mechanical support. A PTFE cell with a 9 mm diameter orifice in the center was tightened to the acrylic base using an O-ring.

Before recording images, substrate tilt corrections were performed by negative feedback line scans in order to obtain  $\Delta_z/\Delta_{x,y} \leq 1.5 \mu\text{m}/\text{mm}$ . Constant substrate potential SG–TC measurements were performed by keeping a constant tip–substrate distance, which is set using a negative feedback approach curve over the Ti plate. The tip and substrate currents were recorded with respect to the tip position in the  $x$ – $y$  plane. In all the imaging modes, the tip was set at  $-0.1$  V versus RHE. When tip shielding was used, the Au layer deposited on the tip walls was also held at  $-0.1$  V (RHE).

Before imaging experiments all the tips were tested by recording approach curves both in 1 mM FcMeOH solution in aqueous 0.1 M KCl (using a silver wire as a quasireference/

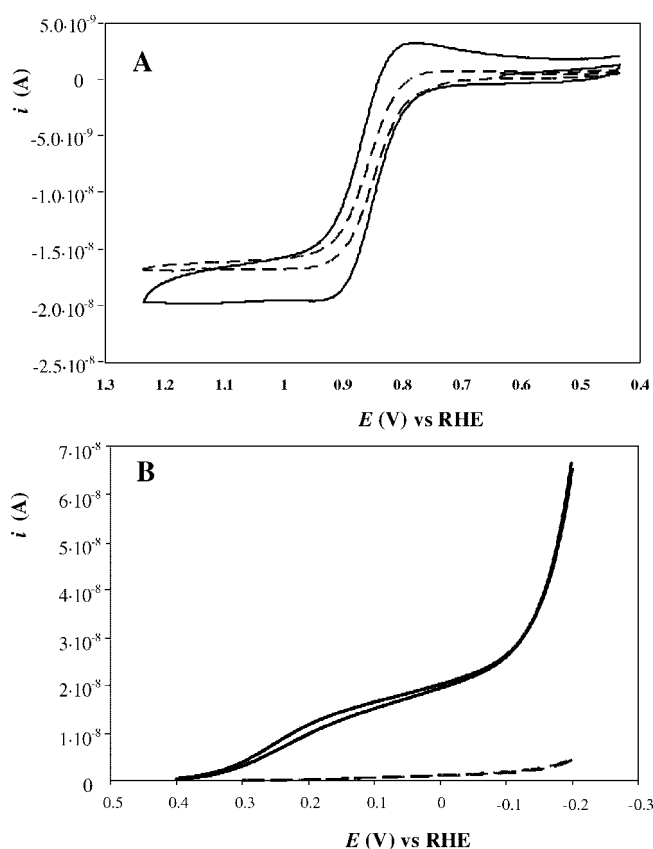


**Figure 3.** Cyclic voltammograms of a 100  $\mu\text{m}$  diam Au tip: (A) in 1 mM FcMeOH + 0.1 M KCl aqueous solution recorded at 10  $\text{mV s}^{-1}$  (—) and 1  $\text{mV s}^{-1}$  (---); (B) in air- (—) and Ar (---)-saturated 0.5 M  $\text{H}_2\text{SO}_4$  aqueous solutions.

counter electrode and a fluorine-doped tin oxide (FTO) substrate placed at  $-0.4$  V for positive feedback and a piece of glass for negative feedback, keeping the tip at 0.6 V in both cases) and in  $\text{O}_2$ -saturated 0.5 M  $\text{H}_2\text{SO}_4$  aqueous solutions. For the latter a tungsten wire and RHE were the counter and reference electrodes, respectively; the substrate consisted of an insulating glass surface.

**Simulations.** The finite element method was used in all simulations. These were performed using the Comsol Multiphysics software. A brief description is given in the Results and Discussion section, and details of the calculations are given in the Supporting Information.

## RESULTS AND DISCUSSION

**Tip Characterization.** We demonstrate the feasibility of a 100  $\mu\text{m}$  diam tip for SECM experiments. The use of a 100  $\mu\text{m}$  diam electrode as an SECM tip is larger than the UMEs usually used to obtain the steady-state behavior necessary for SECM experiments, generally observed for tip radius of about  $a \leq 30 \mu\text{m}$ . However, obtaining steady-state behavior depends on several parameters in addition to the tip radius, e.g., the diffusion coefficient of the reacting species and the time scale of the experiment. Figure 3 shows CV characteristics of a 100  $\mu\text{m}$  diam gold tip in 1 mM FcMeOH (Figure 3A) and in air-saturated aqueous 0.5 M  $\text{H}_2\text{SO}_4$  (Figure 3B) at 1 and 10  $\text{mV s}^{-1}$ . For FcMeOH,<sup>30</sup>  $D = 7.1 \times 10^{-6} \text{ cm}^2 \text{ s}^{-1}$ , the tip does not behave as a UME even at  $\nu = 1 \text{ mV s}^{-1}$  where a significant hysteresis is

(30) Zoski, C. G.; Aguilar, J. C.; Bard, A. J. *Anal. Chem.* **2003**, *75*, 2959–2966.

observed in the CVs (Figure 3A) and the steady-state current ( $i_{ss}$ ) at 0.6 V (ferrocenemethanol oxidation under mass transfer control) is higher than the theoretical  $1.37 \times 10^{-8}$  A, given by eq 1

$$i_{ss} = 4nFcDa \quad (1)$$

where  $n$  is the number of electrons,  $F$  is the Faraday constant,  $c$  is the concentration of the redox species,  $D$  is the diffusion coefficient, and  $a$  is the tip radius. For oxygen ( $D = 1.39 \times 10^{-5}$  cm<sup>2</sup> s<sup>-1</sup>, averaged from data reported in ref 31), the tip characteristics become similar to the steady-state CV expected for a UME. The limiting current in the CV,  $i_{ss} = 2.62 \times 10^{-8}$  A, is in agreement with the theoretical  $i_{ss} = 2.68 \times 10^{-8}$  A (eq 1), with a small residual hysteresis (Figure 3B). In this case the only drawback is the partial overlapping with the hydrogen evolution reaction.

Another important requirement for an SECM tip is that it must follow well-known feedback theory. The tip current as a function of distance toward a surface, an *approach curve*, must match the positive and negative feedback theory for conductive and insulating surfaces, respectively.<sup>32</sup> These approach curves correspond to steady-state measurements of current (expressed as  $I = i/i_{T,\infty}$  where  $i_{T,\infty}$  is the UME steady-state current (eq 1) recorded at a large tip–substrate distance) of a UME approaching a substrate, as a function of dimensionless tip–substrate distance,  $L = d/a$ . An approach curve that fits theory provides the best way to estimate the tip–substrate distance in SECM.<sup>32</sup> Figure 4 shows approach curves obtained in FcMeOH toward a conducting (Figure 4A) and insulating substrate (Figure 4B) and in air-saturated 0.5 M H<sub>2</sub>SO<sub>4</sub> using a 100 μm diam Au tip. Note that under the conditions of the approach curves (Figure 4, both scans performed at 1 μm s<sup>-1</sup>) the currents obtained follow negative and positive feedback theory of steady state quite well. This indicates that even for the case of FcMeOH at the 100 μm diam electrode one can achieve a quasi steady state at sufficiently long times.

In the case of a sulfuric acid medium used in the SECM imaging experiments, the current–distance characteristics obtained with oxygen yields the tip–substrate distance calibration without the need for an additional redox mediator.

**Evaluation of the 100 μm Diameter Tip as an Amperometric Sensor.** The main purpose in using a 100 μm diam tip is to obtain a high collection efficiency, harvesting the highest possible amount of oxygen produced by the spots, even at relatively large tip–substrate distances. A preliminary experiment was conducted imaging a 100 μm diam Au tip in the SG–TC mode to evaluate the collection efficiency at different tip–tip distances. In this experiment, one tip was used to generate O<sub>2</sub> at a constant current of 370 nA and the other tip was used as an amperometric O<sub>2</sub> sensor ( $E_{tip} = -0.1$  V). Figure 5 shows the tip current as a function of its position at three different tip–tip distances. Collection efficiency remained 100% up to a 30 μm tip–tip distance,  $d$ , thus revealing the good behavior of the selected tip as an amperometric sensor for the SG–TC mode.

**Oxygen Evolution Electrocatalysts Screening.** The effectiveness of the shield was first tested using an array of pure

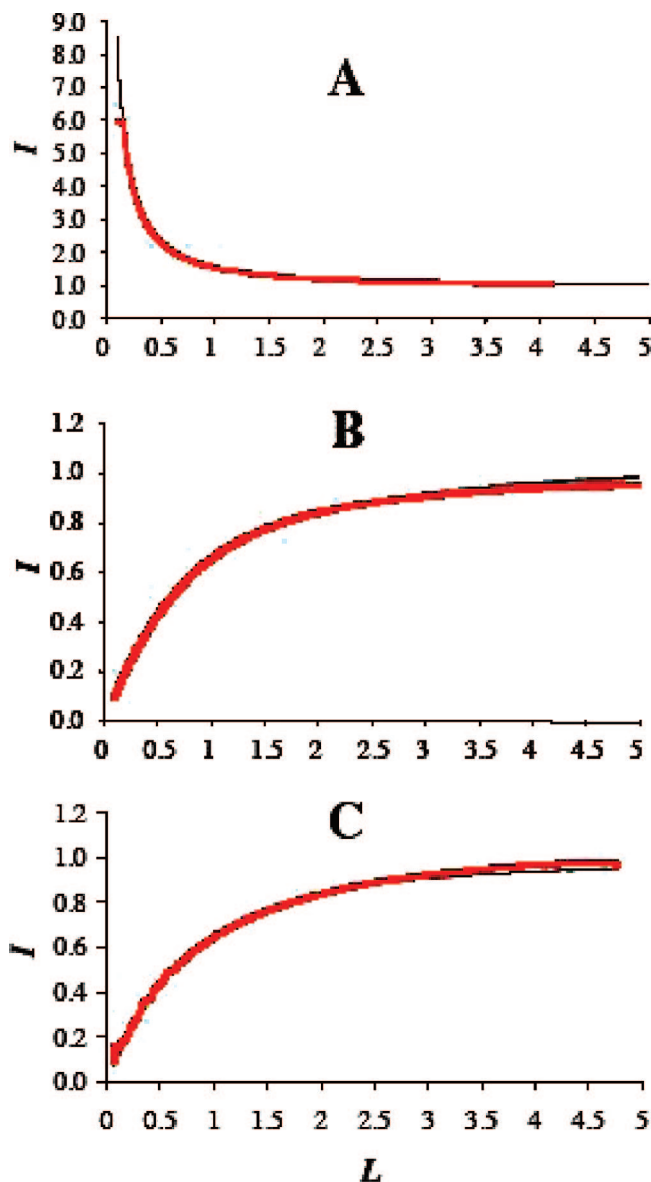


**Figure 4.** Experimental (red lines) and theoretical (black lines) approach curves recorded on a gold 100 μm diam tip (RG = 4) at 1 μm s<sup>-1</sup> under different conditions: line A in 1 mM FcMeOH + 0.1 M KCl aqueous solution using a fluorine-doped SnO<sub>2</sub> on glass electrode as a substrate at -0.4 V vs Ag wire quasireference electrode (positive feedback) or, in line B, over insulating glass (negative feedback); in both (A) and (B)  $E_{tip} = 0.6$  V vs Ag wire quasireference electrode; line C in O<sub>2</sub> (1 atm)-saturated 0.5 M H<sub>2</sub>SO<sub>4</sub> aqueous solution with  $E_{tip} = -0.1$  V vs RHE approaching an insulating (glass) surface as substrate.  $i_{T,\infty}$  of 20.0 nA in (A), 16.0 nA in (B), and 31.6 nA in (C).

IrO<sub>2</sub> spots. In this case, the activity of each spot is the same and the shield is used to obtain a high spot/background contrast in the image. Figure 6 shows the effects of the shield on an SG–TC image in the case of a nine-spot array of IrO<sub>2</sub> spots (sample a) working at the same potential. Because they were prepared in exactly the same way the spots have essentially the same activity and surface area. When the shield is not active or “off”, i.e., the shield is left at open circuit, the contrast is low (Figure 6A) due to the high background current which comes from the accumulation of O<sub>2</sub> being produced at all the catalytic spots. When the shield is turned “on”, i.e., when a potential of -0.1 V versus RHE is applied to reduce oxygen at the shield at a diffusion limited rate

(31) Itoe, R. N.; Wesson, G. D.; Kalu, E. E. *J. Electrochem. Soc.* **2000**, *147*, 2445–2450.

(32) Mirkin, M. V. In *Scanning Electrochemical Microscopy*; Bard, A. J., Mirkin, M. V., Eds.; Marcel Dekker Inc.: New York, 2001; pp 145–199.

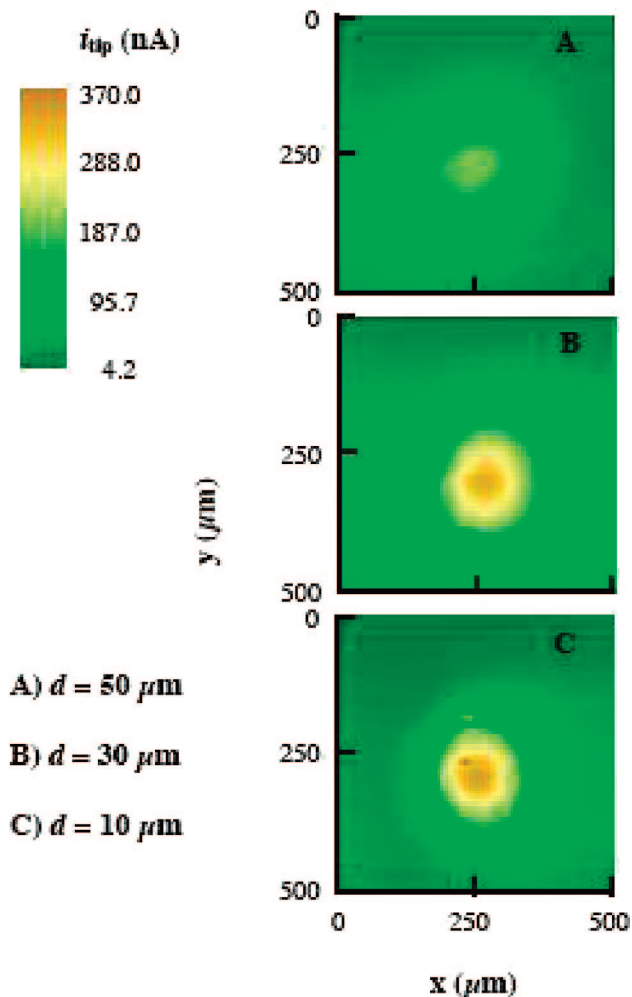


**Figure 5.** SECM images of a Au disk of  $100\ \mu\text{m}$  diam evolving  $\text{O}_2$  at constant current ( $370\ \text{nA}$ ) obtained with a Au disk tip of  $100\ \mu\text{m}$  diam ( $E_{\text{tip}} = -0.1\ \text{V}$  vs RHE) in  $0.5\ \text{M}\ \text{H}_2\text{SO}_4$  at different tip–substrate distances,  $d = 50$  (A),  $30$  (B), and  $10\ \mu\text{m}$  (C). Tip scan rate:  $50\ \mu\text{m}\ \text{s}^{-1}$

(see Figure 3), good contrast between every spot and a lower background is attained (Figure 6B). Note the background in the Figure 6A without the shield ( $\sim 7\ \text{nA}$ ) decreases when the shield is turned on ( $\sim 4\ \text{nA}$ ) as a result of the Au shield consuming the  $\text{O}_2$  around the SECM tip. Note that because of the large distance between spots ( $1000\ \mu\text{m}$  from center to center) and the fact that all the spots show the same activity, all the spots are equally visible. Digital simulations (see below) confirm that the background current is affected by the presence of the spots and that when the shield is set to reduce  $\text{O}_2$ , the background decreases improving the image contrast (Figure 6B).

To test the effectiveness of the shield in the presence of spots showing different activities, array (b) was imaged, which consists of spots with different nominal Ir/Sn atomic ratios. Figure 7 shows an SG–TC image with the shield “off”, i.e., at open circuit (Figure 7A) and with the shield “on” (Figure 7B), i.e.,  $E_{\text{shield}} = -0.1\ \text{V}$  (RHE), with  $E_{\text{subs}} = 1.4\ \text{V}$  (RHE). Note that in the two false color images the current upper and lower limits are the same. In this case, the spots are quite close (around  $200\ \mu\text{m}$  between their boundaries) and the diffusion layers of the spots overlap (Figure 7A). This is also clearly shown in the 3D simulations (see below). This means that in the time it takes to obtain this image (around 45 min), the oxygen concentration between spots is relatively high, thus hampering the image resolution. However, the main draw-

back is that oxygen diffusing from the neighboring spots superimposes on the spot under investigation, distorting the screening of electrocatalytic activity (Figure 7A). The collection efficiency becomes considerably higher than the expected one, as shown below with the simulation results (Figure 9D). The effect is stronger in the case of low-activity spots, since the amount of oxygen produced is comparable with, or even lower than the one coming from the surrounding spots. The use of the tip shield prevents this behavior (Figure 7B). A drawback to using the shield is that it reduces a fraction of the oxygen coming from the spot under investigation, thus lowering the collection efficiency. Nevertheless, using SECM with the tip shield, the evaluation of electrocatalytic activity toward the OER on  $\text{Sn}_{1-x}\text{Ir}_x\text{O}_2$  composites is straightforward. Figure 7B shows clearly that the activity is directly proportional to the Ir content. This confirms that the procedure chosen for varying the Ir/Sn ratio between the spots leads to a progressive change in composition. The absence of strong discontinuities between the spots would rule out surface segregation of the active component, a phenomenon previously observed in the preparation of macroelectrodes.<sup>9,10</sup>

The reliability of the SECM response in array imaging is supported by the slow potentiodynamic measurements (scan rate  $0.167\ \text{mV}\ \text{s}^{-1}$ ) obtained on larger samples (c and d), prepared at two fixed composition, i.e.,  $\text{IrO}_2$  100% and  $\text{IrO}_2/\text{SnO}_2$  60:40,

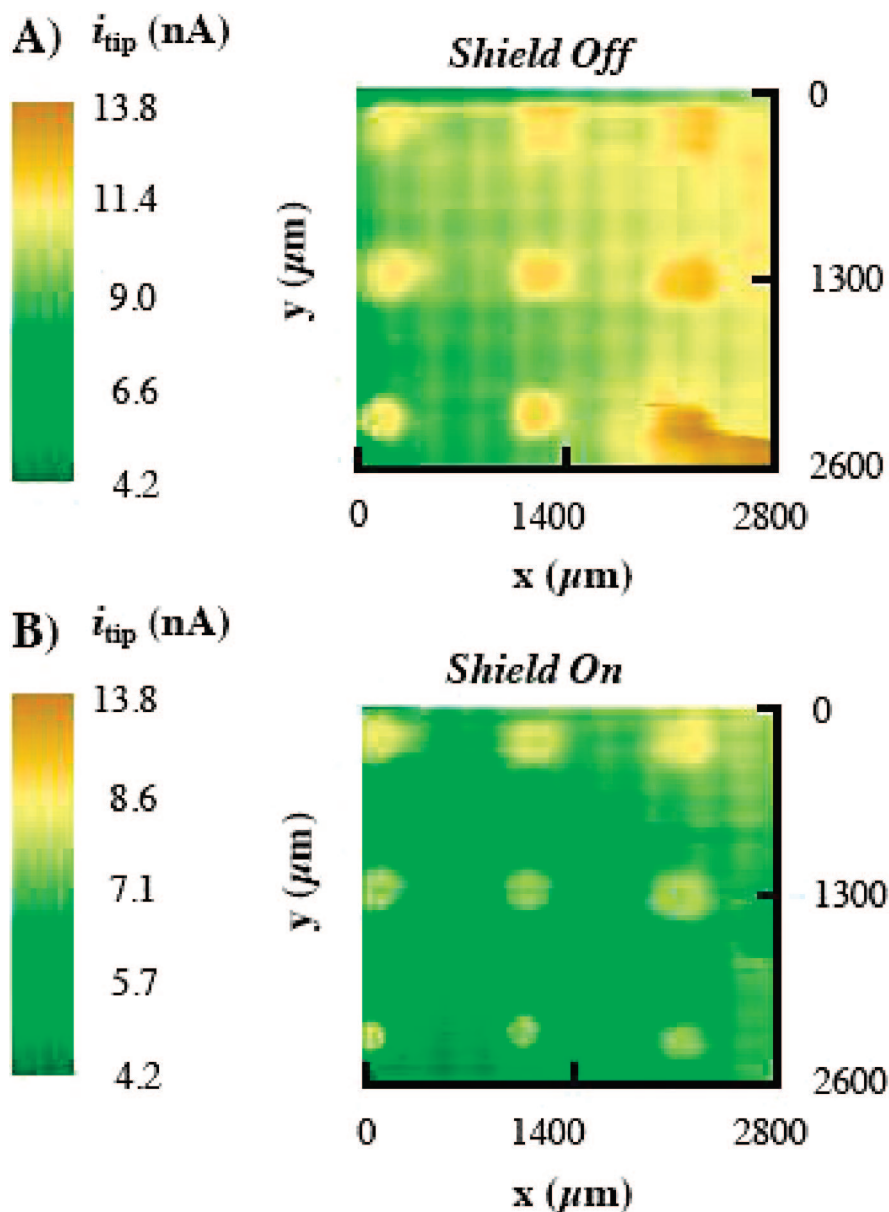


**Figure 6.** SECM images of an array of  $\text{IrO}_2$  particles of  $350 \mu\text{m}$  diam at  $E_{\text{subs}} = 1.4 \text{ V}$  vs RHE in  $0.5 \text{ M H}_2\text{SO}_4$  with the Au shield “off”, i.e., at open circuit (A) and shield “on”: applying a potential of  $-0.1 \text{ V}$  vs RHE (B). Tip–substrate distance,  $d$ , ca.  $20 \mu\text{m}$ . Scan rate  $100 \mu\text{m s}^{-1}$ . Tip  $100 \mu\text{m}$  diam Au disk at  $E_{\text{tip}} = -0.1 \text{ V}$  vs RHE.

respectively. Figure 8 reports the  $E$  versus  $\log(i)$  plots of samples c, d, and of a bare Ti plate; the comparison is meaningful also in terms of currents, since the samples c and d are of the same size and prepared in exactly the same way. The distortion observed in the low-current region ( $\log(i) < -5.5$ ) is attributed to the contribution of the exposed Ti support (to prevent damaging the electrocatalysts, we used an O-ring larger than the spot that exposed some Ti). The Ti exposed is very likely to contribute current due to double layer charging and  $\text{TiO}_2$  layer growth, as shown in the Ti current–potential ( $i$ – $E$ ) curve.

Please note that this  $i$ – $E$  curve for Ti (Figure 8), although of the same geometrical area, corresponds to a larger Ti surface area than the exposed Ti on samples c and d. At higher currents, the linear characteristic is fully recovered for both samples, exhibiting slopes of  $59 \text{ mV/decade}$  for the pure Ir electrode and  $54 \text{ mV/decade}$  for the 60% Ir-containing electrode. These are the typical values obtained on Ir-based electrocatalysts.<sup>9,10</sup> At all potentials,

the sample containing 60% Ir showed lower currents than the pure Ir one. This supports the SECM SG–TC experiments performed on sample b with the shield “on”, which shows a monotonic increase of the current with Ir content (cf., Figure 7B). Compare this to the results with the shield at open circuit, “off” in Figure 7A, which would indicate essentially the same activity for 60% or 100% Ir. Thus, the tip shielding approach correctly reports the trend in electroactivity by removing the interference from neighboring spots.

**SECM Simulations of Tip Shielding.** Three-dimensional diffusion simulations of SECM SG–TC experiments were carried out to obtain a clear picture of the effects of tip shielding, using the COMSOL Multiphysics v.3.2 software (COMSOL, Inc., Burlington, MA), under simulated conditions that resemble the experimental setup used throughout this study. Briefly, the simulation space consisted of an array of  $3 \times 3$  planar active spots of  $300 \mu\text{m}$  diam each, positioned in the  $x$ – $y$  plane and separated

### Sn<sub>1-x</sub>Ir<sub>x</sub>O<sub>2</sub> mixtures nominal composition

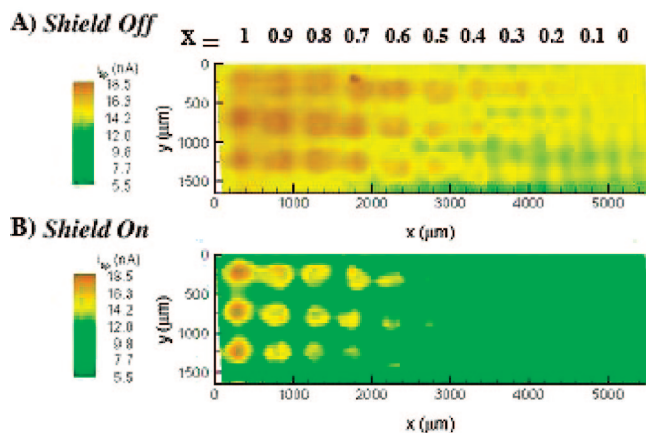


**Figure 7.** SECM images of array of electrocatalytic spots of Sn<sub>1-x</sub>Ir<sub>x</sub>O<sub>2</sub> mixed oxides, nominal  $x$  varying from 1 to 0 with increments of 0.1. Numbers show the atomic percent of Ir on metal basis.  $E_{\text{subs}} = 1.4 \text{ V}$  in  $0.5 \text{ M H}_2\text{SO}_4$  with a  $100 \mu\text{m}$  diam Au tip ( $E_{\text{tip}} = -0.1 \text{ V}$  vs RHE) with the Au shield “off”, at open circuit (A) and “on” applying a potential of  $-0.1 \text{ V}$  vs RHE (B).  $d$  ca.  $35 \mu\text{m}$ . Tip scan rate  $200 \mu\text{m s}^{-1}$ .

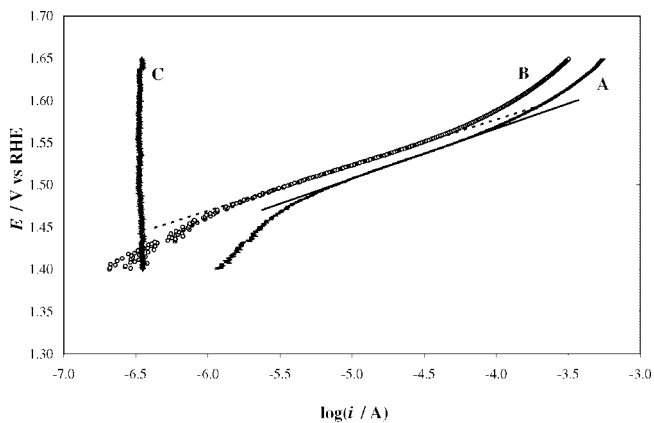


**Figure 8.**  $E$  vs  $\log(i)$  plots at slow scan ( $\nu = 0.167 \text{ mV s}^{-1}$ ) with (curve A,  $\circ$ ) IrO<sub>2</sub> sample c and (curve B,  $\circ$ ) Sn<sub>0.4</sub>Ir<sub>0.6</sub>O<sub>2</sub> sample d obtained with the sol-gel method. Lines show the linear regressions with slopes of 59 and 54 mV/decade for samples c and d, respectively. (curve C,  $+$ ) shows the response of a bare Ti electrode.

by a center-to-center distance of  $500 \mu\text{m}$ . The SECM tip was modeled geometrically as a cone and was positioned below the  $x$ - $y$  plane along the  $z$  axis; the metallic tip diameter was  $100 \mu\text{m}$  and was surrounded by an insulating sheath of  $150 \mu\text{m}$  of radius to give a total tip end face diameter of  $400 \mu\text{m}$ . The tip-to-substrate distance was set to  $30 \mu\text{m}$  in all simulations. Concentration profiles for oxygen in the simulation space were obtained by setting the appropriate boundary conditions: for the metallic tip, a zero concentration boundary was introduced at its surface, whereas for each active spot the generation of oxygen was achieved by setting the diffusive flux to a constant value that corresponded to  $15 \text{ nA}$  of current passed. The initial bulk concentration of oxygen was set to zero, and a diffusion coefficient of  $1.4 \times 10^{-9} \text{ m}^2 \text{ s}^{-1}$  was used to recreate the effect of the tip shielding; the lateral face of the conical tip was set to a boundary condition of zero oxygen concentration, or for comparison, it was left as an insulating boundary. The tip was positioned at different  $x$ - $y$  locations to obtain a lateral scan over the center spot; all

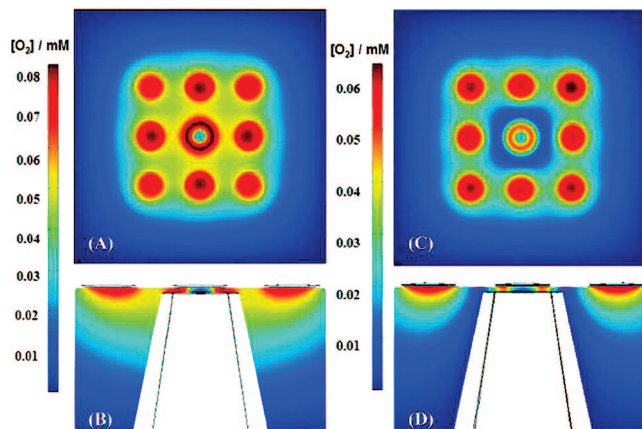


**Figure 9.** Three-dimensional diffusion simulations over a central spot in an array. (A) With the tip shield “off”: top view of the simulation space over the  $x$ - $y$  upper plane, (B) tip shield “off” zoomed in cross section in the  $x$ - $z$  plane through the center of the simulation space. (C) With the tip shield “on”: top view of the simulation space over the  $x$ - $y$  upper plane, (D) with the tip shield “on” zoomed in cross section in the  $x$ - $z$  plane through the center of the simulation space.

calculations were done under steady-state conditions, thus providing a semiquantitative approximation to the real problem in which the raster speed can play a part in the efficiency of the tip shielding. Further details of the simulation are given in the Supporting Information.

Figure 9 shows the result of the simulations for the concentration profiles of oxygen in the array system when the tip is positioned below the center spot. In the case where the conical surface of the tip acts as an insulator and there is no tip shielding, Figure 9, parts A and B, the electrodes communicate through their diffusion layers. An accumulation of the substrate-generated species (oxygen) is readily observed across the array, and thus the collected oxygen at the tip includes contributions not only from the central spot but also from the neighboring ones. Note also that all of the spots interact, and the ones with more neighbors, as the ones located at the centers of the rows and columns, also show a concentration enhancement. It is important to take this effect into account as it leads to an erroneous apparent higher electrocatalytic activity for these center spots. When the tip shielding is turned on, Figure 9, parts C and D, communication between the diffusion layers of neighboring spots is greatly diminished. The region near the edge of the conical tip at its uppermost extreme shows a large decrease in the oxygen concentration. Figure 9D also shows when compared to Figure 9B that there is a decrease in the oxygen concentration inside the tip-substrate gap, mostly due to the concentration gradient induced by the shielding. Although these figures show that the region between the tip sensing electrode and the substrate is substantially less impacted, one must still examine how the tip shielding affects in actual measurements.

Figure 10A shows the collection efficiency (defined as the ratio of the tip current to the central spot current) in a simulated line scan. Notice that the only difference is a vertical displacement in the current efficiency axis. In theory the use of the tip shielding does not greatly affect the behavior of the active part of the tip, but it does free the measurement from the negative effect of the communicating diffusion layers. Because of this, a dramatic reduction of the signal (that ideally would approach zero) is

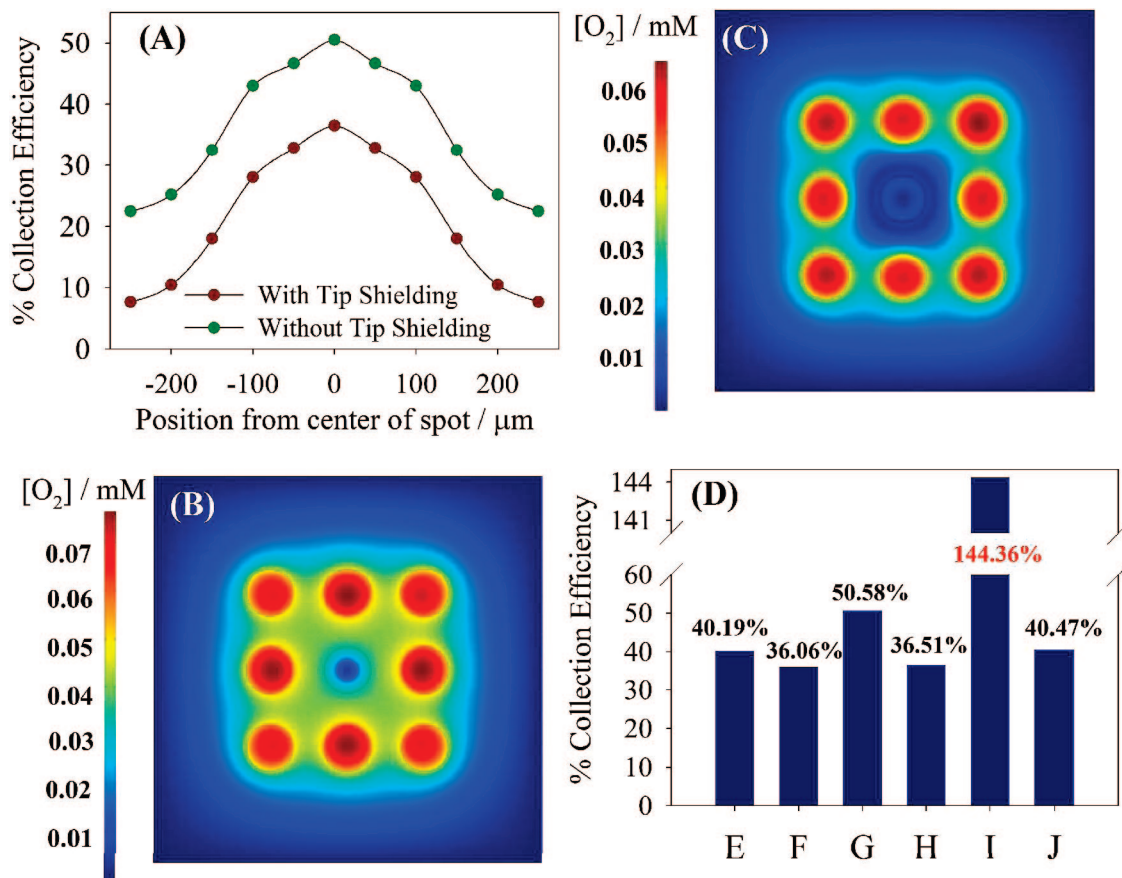


**Figure 10.** (A) Collection efficiency line scans over the central spot at different distances from its center. Top views over the upper  $x$ - $y$  plane for the case when the central spot is only 10% as active as the surrounding spots: (B) without and (C) with tip shielding. (D) Collection efficiency histogram for different simulated conditions: central spot is only active, (E) without and (F) with tip shielding;  $3 \times 3$  array with equal activity on each spot, (G) without and (H) with, tip shielding; central spot is only 10% as active as surrounding spots, (I) without and (J) with tip shielding.

observed in the positions between the spots ( $-250$  or  $250 \mu\text{m}$  in this simulation). Three-dimensional simulation images relevant to Figure 10A are reported in the Supporting Information part S1 and part S2 for a nonshielded tip and for a shielded tip, respectively. Another issue in these experiments is the possibility of having a spot that is of lower activity than the surrounding spots. This case is simulated in Figure 10, parts B and C, where the central spot is only 10% as active as its neighbors. Figure 10B shows that, under these conditions, the diffusion layers of the adjacent spots invade the position of the central spot allowing once again the tip to collect material that is not attributable to the spot directly underneath. When the tip shield is turned on, Figure 10C, the blocking of this transfer is evident, and thus one obtains a less biased measurement. Figure 10D summarizes these results. Bars E and F—relative to the pictures reported in the Supporting Information, part S4, considering a nonshielded tip (Figure S4-i) and a shielded tip (Figure S4-ii)—show the collection efficiency of an isolated spot with the shield “off” (E) and “on” (F); note the collection efficiency decreases when the tip shield is turned on. Bars G and H—relative to the pictures reported in the Supporting Information, considering a nonshielded tip (Figure S1-i) and a shielded tip (Figure S2-i)—show the situation in the simulated  $3 \times 3$  array with equally active spots: (G) shield off; (H) shield on. The collection efficiency of the tip in the shielded case is almost the same for equally active spots (36.5%) with respect to the ideal isolated case (36.1%), showing the effective decrease in the

interference from other spots, whereas the nonshielded case shows a much larger, erroneous increase in the collection efficiency. Finally, the tip shielding method helps avoid wrong measurements as would otherwise occur in the case of an array of nonequal activity of spots, as shown in bars I and J, simulated with a  $3 \times 3$  array with the central spot being only 10% as active as the surrounding spots (see the Supporting Information, part 3, for a nonshielded tip, Figure S3-i, and a shielded tip, Figure S3-ii). An unacceptable value of over 100% collection efficiency is obtained without the shielding (bar I) but yields a closer value (40.5%) to the unbiased situation (36.1%) when the shield is turned on (bar J).

## CONCLUSIONS

A new method for electrocatalyst screening for the OER using SECM is shown. The use of the SG-TC mode combined with a new tip shielding approach is described and demonstrated in studies of oxygen evolution of electrocatalysts. The SECM methodology was applied to arrays of spots of mixed tin + iridium oxides ( $\text{Sn}_{1-x}\text{Ir}_x\text{O}_2$ ,  $0 \leq x \leq 1$ ) on Ti obtained by sol-gel procedure. Experiments were performed in aqueous  $0.5 \text{ M H}_2\text{SO}_4$  and kept under oxygen evolution conditions. In the SG-TC SECM mode, the oxygen produced on each spot is reduced at the tip which is moved along the  $x$ - $y$  plane of the sample. A  $100 \mu\text{m}$  diam tip was selected on the basis of CV and current/tip-substrate distance characteristics (approach curves) that conformed to UME

behavior. Both SECM experiments and digital simulations showed that, during OER electrocatalyst screening, the tip current is a function of the oxygen produced on the spot under investigation but also from the neighboring spots, especially in the case of the lower activity spots in the array, which could lead to error on the interpretation of the electrocatalytic activity of the spots. To avoid this problem, the tip was modified by depositing a thin Au layer on its walls, called the tip shield. When this shield was potentiostatically maintained under oxygen reduction conditions, the tip correctly reported the OER activity of the target spot, being actively shielded from the oxygen produced by the neighboring spots. Both experimental data and simulations support the effectiveness of this methodology.

Finally, when the method was applied to the characterization of  $\text{Sn}_{1-x}\text{Ir}_x\text{O}_2$  arrays, these exhibited direct proportionality between the electrocatalytic activity and the nominal Ir content of the mixed oxide. This trend was confirmed by testing macroscopic samples of known composition with slow potentiodynamic curves. The

combination of the SG–TC SECM mode with the tip shielding approach demonstrated in this article thus provides a powerful new method for testing electrocatalysts by rapid screening.

#### **ACKNOWLEDGMENT**

A.M. thanks The University of Milan (Italy)—Doctorate School in Chemical Sciences and Technologies and FIRST funds. J.R.L. thanks the Secretaría de Educación Pública for a DGRI-SEP Complementary Scholarship. This work was funded by the National Science Foundation (CHE 0451494).

#### **SUPPORTING INFORMATION AVAILABLE**

Additional information as noted in text. This material is available free of charge via the Internet at <http://pubs.acs.org>.

Received for review January 17, 2008. Accepted March 24, 2008.

AC8001287